IMPROVEMENT OF COBRA-TF CODE MODELS FOR LIQUID ENTRAINMENTS IN FILM-MIST FLOW

July 1993

Alexandre EZZIDI*, Tsutomu OKUBO
and Yoshio MURAO

日 本 原 子 力 研 究 所
Japan Atomic Energy Research Institute

Improvement of COBRA-TF Code Models

for Liquid Entrainments in Film-mist Flow

Alexandre EZZIDI[*], Tsutomu OKUBO and Yoshio MURAO

Department of Reactor Engineering

Tokai Research Establishment

Japan Atomic Energy Research Institute

Tokai-mura, Naka-gun, Ibaraki-ken

Based on the investigation on the previous studies, correlations for the entrainment and deposition have been changed in the COBRA-TF code in order to improve its predictive capability for the entrainment/deposition phenomenon at low pressures less than 0.5 MPa.

As the first step, Sugawara's correlations for the entrainment and the deposition were introduced into COBRA-TF. The calculational results with these became in much better agreement with the concerned experimental data than before, but the agreement was not yet satisfactory. Then, as the second step, the correlation for the interfacial friction factor was also changed to the Wallis' and this resulted in some more improvement in the calculational results. However, discrepancies between calculated results and the experimental data were still in the range of about 20%.

In order to get a better agreement with the experimental data, a new entrainment correlation has been derived based on the Würtz's correlation and the Sugawara's for modification factors. The new correlation has one more factor than the Sugawara's and this factor is a function of two Reynolds numbers for the liquid film and the relative

---

* An STA Fellow during May, 1992 - May, 1993

motion between the vapor and the liquid film. The calculated results with the new entrainment correlation together with the Sugawara's deposition correlation and the Wallis' interfacial friction factor correlation are in excellent agreement with the experimental data in a wide range of flow conditions, indicating a significant improvement on the predictive capability of COBRA-TF for the entrainment/deposition phenomenon.

COBRA-TFコードの液膜噴霧流に対する
エントレインメントモデルの改良

日本原子力研究所東海研究所原子炉工学部
Alexandre EZZIDI*・大久保　努・村尾　良夫

　0.5 MPa以下の圧力下での液滴の発生・沈着現象に対するCOBRA-TFコードの予測能力を改善するため、コードで使用されている液滴の発生および沈着の相関式について検討した結果に基づいて、新しい相関式を導出した。

　第1段階として、液滴の発生および沈着に対する菅原の相関式をCOBRA-TFに導入した。これらを用いた計算の結果は、参照した実験データに対して以前の結果に比べてはるかに良好な一致を示すようになったものの、一致の程度はまだ不十分であった。第2段階として、更に相関摩擦係数に対する相関式もWallisのものに変更した。その結果、より良好な結果が得られたが、実験値と計算値の間には、まだ20％程度の相違があった。

　そこで、実験データとのより良い一致を得るため、Würtzの相関式と菅原のそれに対する補正因子の考えに基づいて、液滴の発生に対する新たな相関式を導出した。この新相関式は、菅原の相関式に更にもう一つの因子を付加したものであり、この因子は、液膜の流動並びに蒸気と液膜の相対的な流動に対する2つのレイノルズ数の関数になっている。液滴の発生に対する新相関式に加え、液滴の沈着に対する菅原の相関式およびWallisの相関摩擦係数相関式を用いて得られた計算結果は、広い範囲の流動条件下で実験データと非常に良好な一致を示し、液滴の発生・沈着現象に対するCOBRA-TFコードの予測能力が大きく改善された。

東海研究所：〒319-11　茨城県那珂郡東海村白方字白根2-4

＊原子力交流制度研究員（1992年5月～1993年5月）

Contents

目　　　　次

1. Introduction

The COBRA-TF (Coolant Boiling in Rod Arrays, Two-Fluid) computer code[1] was developed at the Pacific Northwest Laboratory in the USA to provide best estimate thermal hydraulic analysis of a Light Water Reactor (LWR) core for design basis accidents and anticipated transients. It is the final version of the COBRA family subchannel analysis codes[2],[3].

The most important feature in COBRA-TF is it provides a two-fluid three-field representation of two-phase flow, instead of the homogeneous representation used in the previous versions of the COBRA codes, such as COBRA-IV-I[2]. The three fields are : continuous vapor, continuous liquid and entrained liquid. Therefore, the code is appropriate to be utilized to analyze the film-mist flow behavior, which we are interested in from the point of view of the prediction of the film dryout phenomenon expected in the reactor core. The code also features extremely flexible noding for both the hydrodynamic and the heat transfer solution. This flexibility provides the capability to model the wide variety of geometries encountered in components of nuclear reactor primary system. Furthermore, COBRA-TF can be used with either subchannel or rectangular cartesian coordinates, which allows a fully three dimensional treatment.

To close the equation set for the two-phase flow, some physical models are needed for the mass and momentum exchange among the three fields at the phase interfaces, the drag forces at solid boundaries, knowledge of the turbulence terms in the continuous fields and so forth. Since we are particularly interested in the precise prediction of the critical heat flux or the film dryout phenomenon in the reactor core, the physical models related to the liquid entrainments in the film-mist flow used in the COBRA-TF code have been investigated and assessed with some basic experimental data in order to clarify the predictive capability of COBRA-TF for the basic entrainment/deposition phenomenon in the film-mist flow. The essential features of the film-mist flow are that the vapor travels in the center of the flow channel, i.e. the subchannel, the liquid film travels on the fuel rod surfaces and the liquid droplets are carried along with the vapor flow. These droplets are continually torn from the liquid film by the break-up of the crests of disturbance waves at the vapor-liquid interface[4]. On the other hand, simultaneously, the droplets deposit on the liquid film by the impingement on the rods. When the liquid film flow rate approaches zero due to heat release from the fuel rods and it finally vanishes, the dryout occurs. Therefore, in diabatic flows, liquid entrainment and deposition are of critical importance in modeling heat and mass transfer processes.

The detailed investigation previously made by the authors[5] on the entrainment and

deposition models used in COBRA-TF indicated the following :

(1)   The code can predict the entrainment flow rate well under high pressures of 3.4 and 6.9 MPa, but not under low pressures of 0.24 ~ 0.45 MPa. Figures 1.1 through 1.3 show these results.

(2)   The main reason for the discrepancies at low pressures shown in Fig. 1.3 is considered to that the Würtz's entrainment correlation[6] used in the code, which was developed mainly based on his experimental data obtained at high pressures of 3 to 9 MPa, is not suitable for low pressure situations.

(3)   Sugawara's correlations[7] used in the FIDAS code[8] are promising to improve the predictive capability of the code, since they can take account of low pressure situations.

The objective of this study is to improve the entrainment and deposition models in the COBRA-TF code based on the above information from the previous study. The improvements have been performed on the basis of assessment calculations for the basic experiments conducted by Hewitt et al.[9],[10] with the steam-water two-phase flow flowing in a simple tube under adiabatic conditions.
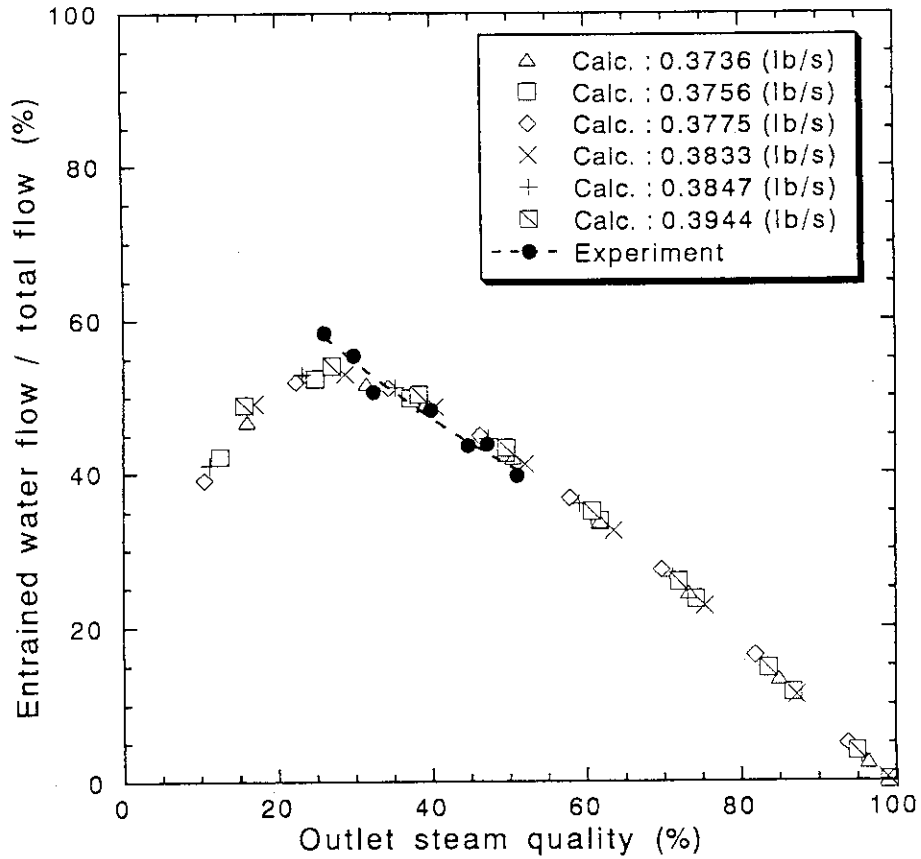
Fig. 1.1   Comparison of entrainment percentage out of total flow between calculation and experiment for 3.4 MPa (500 psia) case[5]
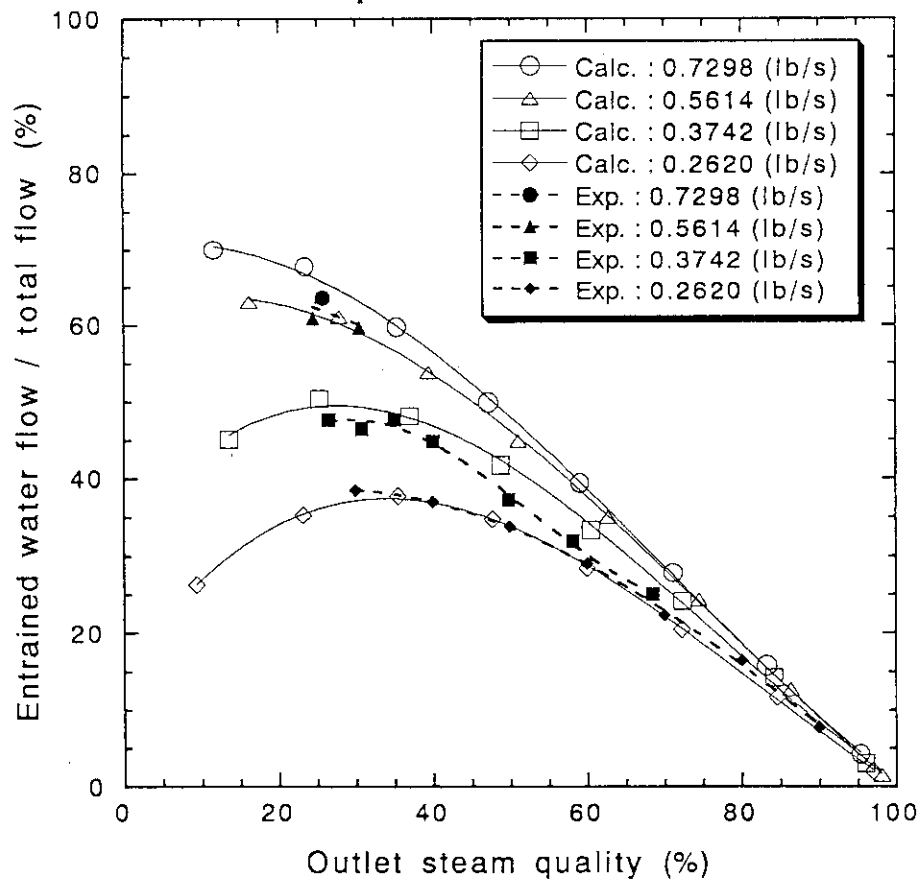

Fig. 1.2   Comparison of entrainment percentage out of total flow between calculation and experiment for 6.9 MPa (1000 psia) case[5]
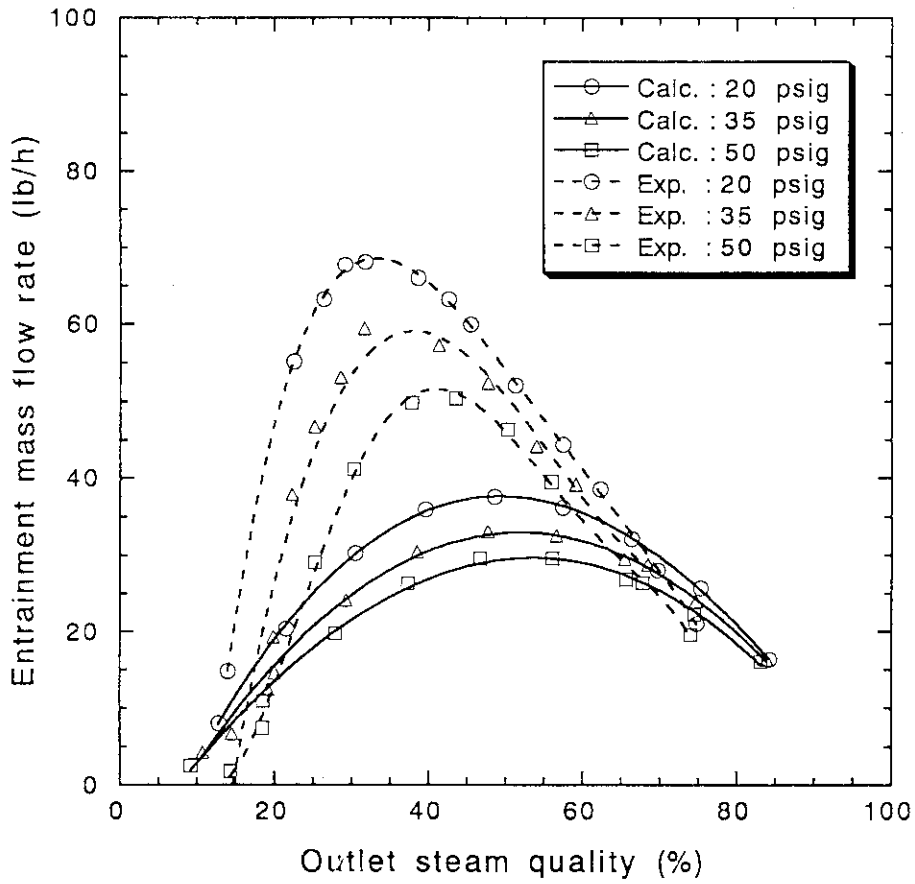
Fig. 1.3　Comparisons of entrainment mass flow rate between calculation and experiment for lower pressures[5]

2. Physical Models for Entrainment and Deposition for Film-Mist Flow

2.1 General Description for Two-phase Flow Models in COBRA-TF

The two-fluid three-field representation is considered to be the most convenient and physically reasonable way to handle flows where the liquid coexists in both continuous (film) and discrete (droplet) forms as appears in the film-mist flow. This formulation uses a separate set of conservation equations (Mass, Energy, and Momentum) for each field. Therefore, this two-fluid three-field description of two-phase flow results in a set of nine equations in general. In addition, the COBRA-TF code can treat the noncondensible gas mixture such as air, nitrogen and so forth. In the COBRA-TF code, four mass conservation equations are used for the vapor, continuous liquid, entrained liquid and noncondensible gas mixture. Three momentum equations are solved allowing the two liquid fields to flow with different velocities relative to the vapor phase. They are described in either the three-dimensional form or the subchannel form. Two energy conservation equations, in which the continuous liquid and the entrained liquid are assumed to be at the same temperature, are specified for the vapor-gas mixture and the combined liquid fields. These conservation equations are solved using a semi-implicit finite-difference numerical technique on an Eulerian mesh.

In the COBRA-TF code, two types of flow regimes are considered[1]. One is named "normal" flow regime and is illustrated in Fig. 2.1. The other is named "hot wall" flow regime and illustrated in Fig. 2.2. The latter is prepared for a detailed analysis of reflooding phenomena expected to appear during the large-break loss-of-coolant accident and is automatically selected in the calculation when a mesh cell contains a solid surface with a temperature greater than 750 °F (672 K).

In the present study, only the "normal" flow regime is concerned. Figure 2.3 summarize the detailed flow regime selection logic for the "normal" flow regime. As presented in Figs. 2.1 and 2.2, entrainment is possible to exist at the void fraction over 0.5, where the flow regime is referred to as churn-turbulent flow. This flow regime is actually defined as a linear interpolation area between the slug flow and the film-mist flow. Transition from the churn-turbulent flow to the film-mist flow is defined as that the void fraction is over a critical value presented in the following :

$$\alpha_{v_{crit}} = \max(\, 1 - \alpha_{l_{crit}}\, ,\, 0.8\,) \qquad (1)$$

$\alpha_{l_{crit}}$: critical liquid volume fraction defined in Eq.(6)

As described in the following, liquid film is considered to be stable in the film-mist flow and to be unstable in the churn-turbulent flow.

In the following, physical models used in COBRA-TF for the liquid entrainment and deposition in the film-mist flow are presented. They are exactly based on the information obtained from the FORTRAN statements for COBRA-TF and presented in British units expression as in the code. Therefore, "nomenclature" of this report is also given in British units.

2.2 Entrainment Model for Film-Mist Flow

The entrainment generation rate S_E is calculated in COBRA-TF by using Würtz empirical correlation[6] and it is expressed as follows :

$$S_E = 0.41 \left(\frac{k_s \times \tau_i}{\sigma} \right) \left(\frac{u_v \times \mu_l}{\sigma \times g} \right) P_w \times \Delta x \tag{2}$$

k_s : equivalent sand roughness
τ_i : shear stress at vapor-liquid interface
u_v : vapor axial velocity
μ_l : liquid dynamic viscosity
σ : surface tension of liquid
g : gravitational acceleration
P_w : wetted perimeter
Δx : axial mesh length

where, k_s is expressed in the form :

$$k_s = 0.57 \, \delta_{th} + 6.625 \times 10^3 \, \delta_{th}^2 - 3.56 \times 10^6 \, \delta_{th}^3 + 1.5736 \times 10^9 \, \delta_{th}^4 \tag{3}$$

where, theoretical film thickness δ_{th} is defined as :

$$\delta_{th} = \frac{D_h \times \alpha_l}{4} \tag{4}$$

D_h : hydraulic diameter
α_l : liquid volume fraction

The shear stress at the vapor-liquid interface is calculated as follows :

$$\tau_i = f_i \times \rho_v \times u_{vl}^2 / (2 \times g) \tag{5}$$

ρ_v : vapor density
u_{vl} : relative velocity between vapor and liquid fields

where the friction factor f_i is given as in the following depending on whether the film flow is stable or unstable. In the code, the liquid film is assumed to be stable when :

$$\alpha_l < \alpha_{l_{crit}} = \frac{2 \times \sigma \times g}{D_h \times \rho_v \times u_{vl}^2} \qquad (6)$$

Otherwise, the liquid film is assumed to be unstable. For the stable film flow, friction factor f_i is given by Wallis correlation[11] as follows :

$$f_{iW} = 0.005 \times \left(1 + 75 \times \alpha_l \right) \qquad (7)$$

This correlation is used in the code not only for the stable film but also for the unstable film flow when solving the transverse momentum equations. When solving the vertical momentum equations for the unstable film flow, the friction factor is given as follows :

$$f_i = \max \left(f_{iH}, 5 \times f_{iW} \right) \qquad (8)$$

where, f_{iW} is given by Eq. (6) above and f_{iH} is given by Henstock and Hanratty correlation[12], which is expressed as follows :

$$f_{iH} = f_s \times \left(1 + 1400 \times F \times \left\{ 1 - \exp \left[-\frac{1}{G} \times \frac{(1 + 1400 \times F)^{3/2}}{13.2 \times F} \right] \right\} \right) \qquad (9)$$

$$G = \frac{\rho_l \times g \times D_h}{\rho_v \times u_v^2 \times f_s} \qquad (10)$$

$$F = \frac{m^+}{Re_v^{0.9}} \times \frac{\mu_l}{\mu_v} \times \left(\frac{\rho_v}{\rho_l} \right)^{\frac{1}{2}} \qquad (11)$$

$$m^+ = \left[\left(0.707 \times Re_l^{0.5} \right)^{2.5} + \left(0.0379 \times Re_l^{0.9} \right)^{2.5} \right]^{0.40} \qquad (12)$$

$$f_s = 0.25 \times \max \left(1.691 / Re_v^{0.43}, 0.117 / Re_v^{0.14}, 64 / Re_v \right) \qquad (13)$$

ρ_l : liquid density
Re : Reynolds number

The size of droplets formed by entrainment from liquid films has been characterized by Tattarson et al.[13]. His results are used in the code and the diameter of droplets is given

by

$$d = 0.0112 \left(\frac{D_h \times \sigma \times g}{\frac{f_s}{2} \times \rho_v \times u_{vi}^2} \right)^{0.5} \tag{14}$$

$$f_s = 0.046 \, Re_v^{-0.20} \tag{15}$$

2.3 Deposition Model for Film–Mist Flow

The deposition of liquid droplets on the liquid film is due to random turbulent motions that impart transverse velocity to the drops, bringing them into contact with the liquid film. The code uses Cousin's expression[14] to determine the deposition rate S_{DE} :

$$S_{DE} = k_D \times C \times P_w \times \Delta x \tag{16}$$

where, C is the mean droplet concentration in the vapor core as given by the expression :

$$C = \frac{\alpha_e \times \rho_l}{\alpha_e + \alpha_v} \tag{17}$$

α_e : entrainment volume fraction

α_v : vapor volume fraction (normally, void fraction)

and k_D is the mass transfer coefficient, which has been found[15] to be a function of surface tension and is expressed in the code as :

$$k_D = \max \left(3.0491 \times 10^{12} \times \sigma^{5.3054} , \; 12.491 \times \sigma^{0.8968} \right) \tag{18}$$

In the equilibrium situation, the rate of entrainment of the droplets from the liquid film is equal to the rate of deposition of droplets back into the film. That is,

$$S_E = S_{DE} = k_D \times C_{eq} \times P_w \times \Delta x \tag{19}$$

Film / film-mist flow

Stable film flow

$\alpha_v = \alpha_{v_{rt}}$

Unstable film flow

Churn-turbulent flow
(linear interporation area)

$\alpha_v = 0.5$

Onset of entrainment
generation

Small bubbles dispersed in
liquid at a volume fraction of 0.2

Slug flow

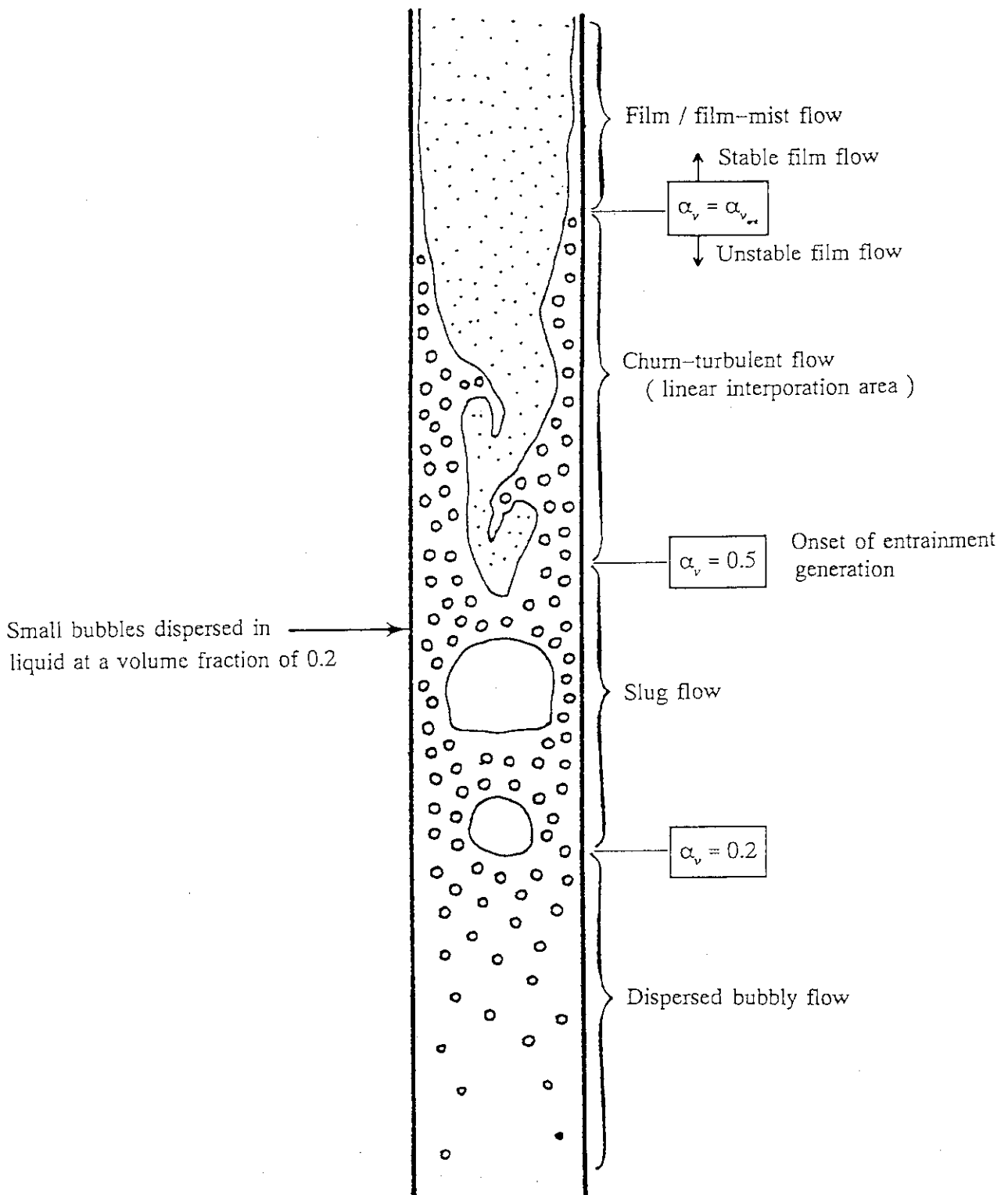$\alpha_v = 0.2$

Dispersed bubbly flow
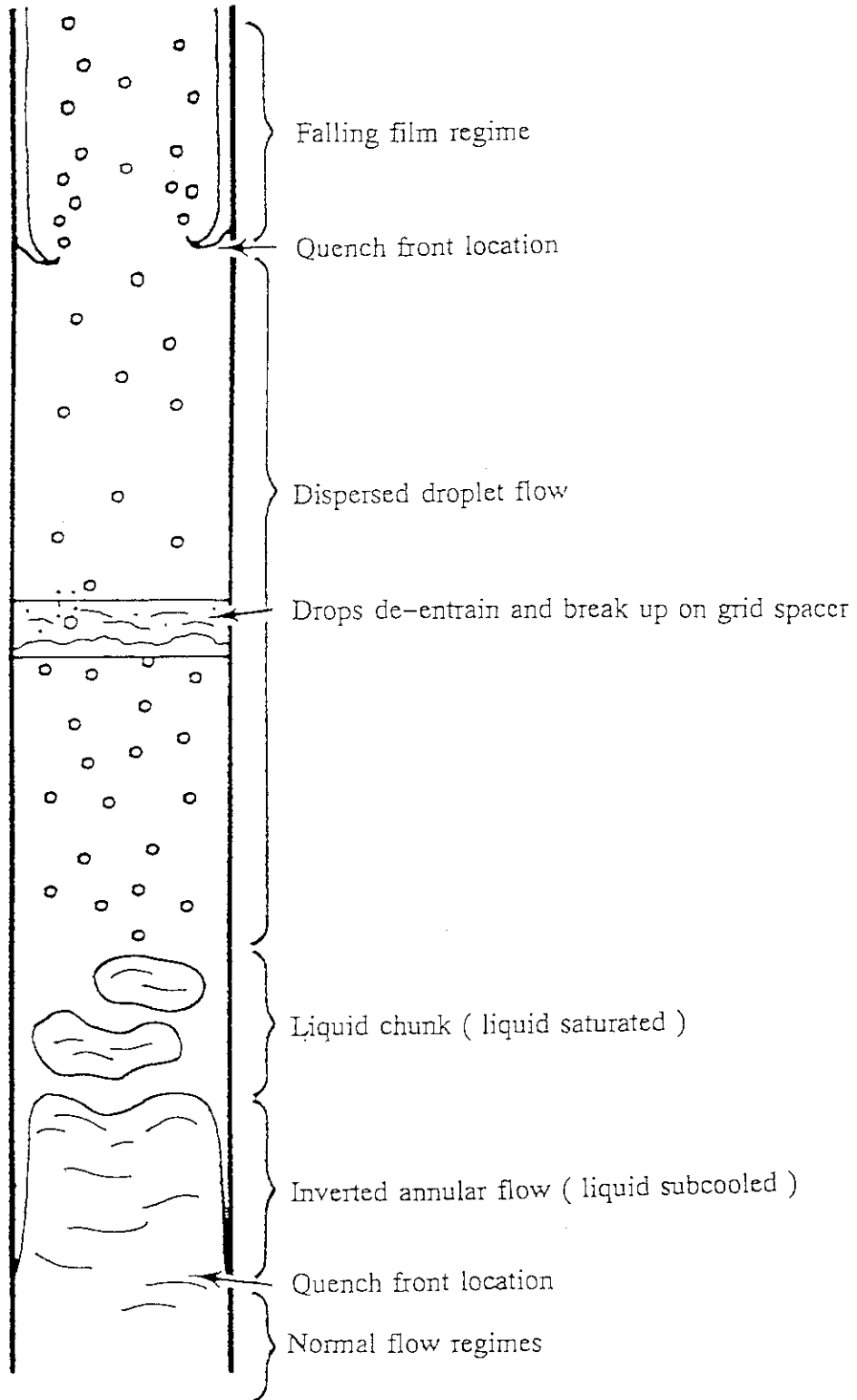
Fig. 2.1　Normal two-phase flow regimes
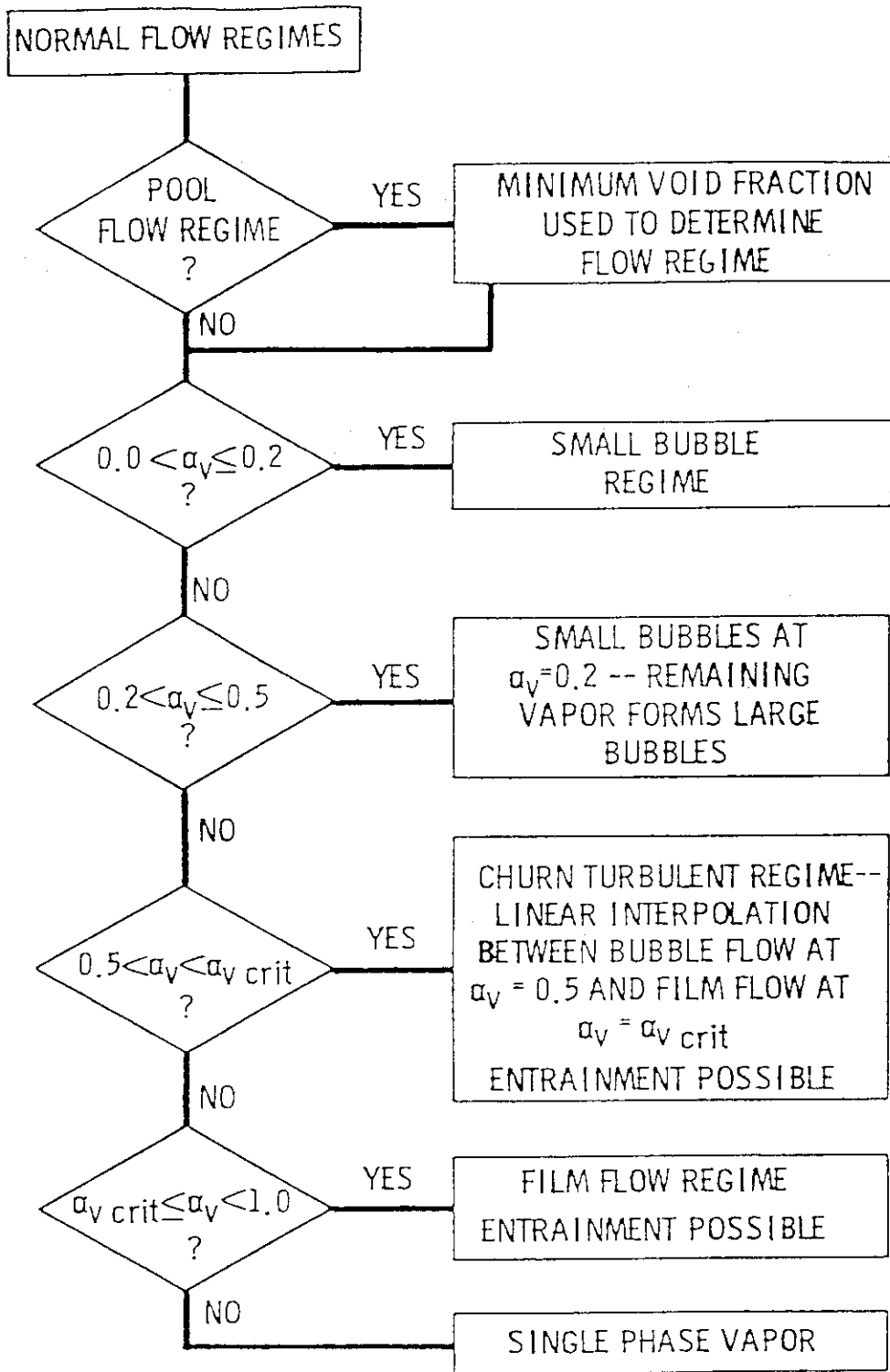
Fig. 2.2   Hot wall flow regimes

Fig. 2.3   Normal flow regime selection logic

3. Assessment Calculations with Sugawara's Models

3.1 Expression of Sugawara's Models in COBRA-TF Code

The previous study[5] on entrainment/deposition models used in COBRA-TF code has indicated that the models are not suitable for low pressure and low mass flow rate situations and that new droplet entrainment and deposition models developed by Sugawara[7] are promissing to improve the calculational results. The capabilities of these new models were successfully demonstrated[7] by comparisons between the calculations using his subchannel analysis code FIDAS[8] and the measurements from some experiments including those of Hewitt et al.[9] and Keeys et al.[10]. Therefore, his models are introduced into COBRA-TF in order to improve it. They are presented in the following in british units.

The entrainment generation rate m_E is as follows :

$$m_E = 0.219 \times \left(\frac{\Delta h_{eq} \times \tau_l}{\sigma} \right) \times \left(\frac{u_v \times \mu_l}{\sigma \times g} \right) \times \left(\frac{\rho_l}{\rho_v} \right)^{0.4} \tag{20}$$

where, Δh_{eq} is the hydrodynamic equivalent wave height and is expressed with the equivalent sand roughness k_s defined in Eq.(3) :

$$\Delta h_{eq} = k_s \quad , \qquad\qquad\qquad for\ Re_v > 1 \times 10^5 \tag{21}$$

$$\Delta h_{eq} = k_s \times \left[2.136 \times \log_{10}(Re_v) - 9.68 \right] \quad , \qquad for\ Re_v \le 1 \times 10^5 \tag{22}$$

The deposition rate m_{DE} is expressed as follows :

$$m_{DE} = 9.0 \times 10^{-3} \times \left(\frac{C}{\rho_v} \right)^{-0.5} \times Re_v^{-0.2} \times Sc^{-2/3} \times u_v \times C \tag{23}$$

These models were expressed in COBRA-TF in the following forms :

Entrainment generation rate :

$$S_E = 0.219 \times \left(\frac{\Delta h_{eq} \times \tau_l}{\sigma} \right) \times \left(\frac{u_v \times \mu_l}{\sigma \times g} \right) \times \left(\frac{\rho_l}{\rho_v} \right)^{0.4} \times P_w \times \Delta x \tag{24}$$

Deposition rate :

$$S_{DE} = 9.0 \times 10^{-3} \times \left(\frac{C}{\rho_v}\right)^{-0.5} \times Re_v^{-0.2} \times Sc^{-2/3} \times u_v \times C \times P_w \times \Delta x \tag{25}$$

Sc is the Schmidt number and can be calculated[7] using Lewis relation $Sc \approx Pr$, where Pr is the vapor Prandtl number. The other parameters are defined in Eq.(2).

3.2 Calculational Results with Sugawara's Models

In the same way as the previous study[5], assessment calculations were performed by simulating the same basic entrainment/deposition experiments as before. They were conducted by Hewitt et al.[9] and Keeys et al.[10] with a simple tube test section under adiabatic conditions and were also used by Sugawara for the development of his correlations[7]. The geometrical parameters of the test section are given in Table 3.1 for each experiment. The test section was modeled in a single subchannel treatment with some appropriate boundary conditions given at the inlet and the outlet of the test section as in the previous study[5]. The thermal hydraulic parameters used in the calculations are summarized in Tables 3.2 and 3.3. The steam quality was varied over the range of 10 to 90 %. The channel noding diagram employed in the calculations is given in Fig. 3.1. The calculations were made by simply replacing the entrainment and deposition correlations in COBRA—TF, which are expressed in Eqs.(2) and (16), with Sugawara's correlations expressed in Eqs.(24) and (25).

The calculational results of the entrained liquid mass flow rate and the percentage of the entrainment out of the total flow are summarized in Tables 3.4, 3.5 and 3.6 for the low pressures of 20, 35 and 50 psig, respectively, and in Table 3.7 for the high pressure case of 500 psia. These results are plotted against the exit steam quality in Figs. 3.2 and 3.3, respectively. They show that COBRA—TF results are more than 20 % higher for low pressures and slightly higher for high pressure. On the contrary, in the calculations[7] made by Sugawara using the FIDAS code, the entrainment flow rates roughly coincided with the experimental data.

3.3 Effects of Interfacial Friction Factor

One possible reason for the discrepancy in the above results is that the film flow was assumed to be unstable in COBRA—TF calculations[5], and hence, the interfacial friction factor was five times higher than the values calculated with Wallis correlation as in Eq.(8), i.e. $f_i = 5 \times f_{iW}$. However, Sugawara's entrainment correlation was established[7] together with the Wallis friction factor without any multiplication, i.e. $f_i = f_{iW}$. Since this difference is

considered to give a significant effect, a second series of calculations was made using the Wallis correlation expressed in Eq.(26) as in the FIDAS calculations.

$$f_{iW'} = \frac{1}{4} \times \left(\frac{0.316}{Re_v^{0.25}} \right) \times \left(1 + 300 \times \frac{\delta_{th}}{D} \right) \tag{26}$$

D : diameter

Calculational results are summarized in Tables 3.8 through 3.11 and are plotted in Figs. 3.4 and 3.5. They show a slight decrease in the entrainment flow rate comparing with Figs. 3.2 and 3.3, but the calculated results are still higher by about 20 % than the experimental data. This will be discussed in the next section.

3.4 Discussion on Calculated Results with Sugawara's Models

Since the entrainment generation rate is proportional to the interfacial friction factor as described in Eqs.(24) and (5), the multiplication factor of five used in the first series of calculations is considered to have a significant effect on the calculational results. Calculation-al results presented above, however, are only slightly different from the other series of calculations presented in Sec. 3.2. This suggests that other effects of the interfacial friction factor on the two–phase flow calculation are significant and diminish the proportional dependency mentioned above. This effect should be noted when the interfacial friction factor is selected.

Sugawara developed his entrainment correlation based on the Würtz's correlation by introducing additional two factors of the density ratio, which takes account of the pressure effect, and the vapor Reynolds number, which is considered to include both the pressure and the mass flux effects. In order to establish these factors, he used[7] the experimental data from Hewitt et al.[9],[10]. However, since there was no direct experimental data for the entrainment generation rates (m_E), the experimental data he utilized are considered to be the estimated values obtained through the FIDAS code with his deposition correlation. Therefore, it is not certain that the correlation can apply directly to COBRA–TF, which has the different code structure from FIDAS. That is, the entrainment and deposition phenomena are not determined only by the entrainment and deposition correlations, but by the flow situation of the liquid film and the vapor, which is affected also by other physical models and ways to treat individual phenomenon. Judging from the results presented above, these effects seem to be rather large and the two additional factors might not be enough for the COBRA–TF code. This suggests a necessity of modification on Sugawara's entrainment correlation.

Table 3.1 Geometrical parameters for input

Geometrical parameters		Hewitt *et al.*	Keeys *et al.*
Nominal channel flow area	(in²)	0.1052	0.1940
Channel wetted perimeter	(in)	1.150	1.561
Intside diameter of tube	(in)	0.366	0.497
Total lenght of tube	(in)	144.0	144.0

Table 3.2 Thermal hydraulic parameters for Hewitt *et al.* experiments

X	Inlet Fluid Enthalpy (Btu/lb)						
	P=20	P=25	P=30	P=35	P=40	P=45	P=50
10	321.43	329.05	335.93	342.21	348.01	353.42	358.59
20	415.38	422.44	428.81	434.63	439.99	444.98	449.64
30	509.32	515.82	521.69	527.04	531.96	536.54	540.81
40	603.27	609.21	614.57	619.45	623.94	628.10	631.98
50	697.21	702.60	707.46	711.87	715.91	719.65	723.15
60	791.16	795.98	800.34	804.27	807.89	811.21	814.31
70	885.09	889.39	893.23	896.70	899.85	902.77	905.49
80	979.03	982.76	986.10	989.10	991.83	994.33	996.66
90	1072.98	1076.15	1078.41	1081.52	1083.81	1085.89	1087.83

X : Inlet quality (%)
P : Outlet pressure (psig)
G : Total mass flow rate = 0.04445 (lb/s)

Table 3.3 Thermal hydraulic parameters for Keeys *et al.* experiments

Inlet Fluid Enthalpy (Btu/lb)

X	P = 500 psia, T = 435.6 °F						P = 1000 psia, T = 545.0 °F			
	G=0.3736	G=0.3756	G=0.3775	G=0.3833	G=0.3847	G=0.3944	G=0.2620	G=0.3742	G=0.5614	G=0.7298
20	570.84	544.16	528.96	578.36	533.84	568.24	603.60	630.64	648.52	618.72
30	687.86	637.89	619.09	666.94	625.11	653.96	693.40	707.06	724.08	695.88
40	744.88	731.62	709.22	755.52	716.38	739.68	773.20	783.48	799.64	773.04
50	831.90	825.10	799.35	844.10	807.65	825.40	853.00	859.90	875.20	850.20
60	918.92	919.08	889.48	932.68	898.92	911.12	932.80	936.32	950.76	927.36
70	1005.94	1012.81	979.61	1021.26	990.19	995.94	1012.60	1012.74	1026.32	1004.52
80	1092.96	1106.54	1069.74	1109.84	1081.46	1082.56	1092.40	1089.16	1101.88	1081.68
90	1179.98	1200.27	1159.87	1198.42	1172.73	1168.28	1172.20	1165.58	1177.44	1158.84

X : Inlet quality (%)
P : Outlet pressure (psia)
T : Saturation temperature (°F)
G : Total mass flow rate (lb/s)

Table 3.4 Calculated entrainment mass flow rate and percentage with $f_i = 5 \times f_{iw}$
Outlet pressure : <u>20</u> (psig) , Total mass flow rate : <u>0.04445</u> (lb/s)

Outlet Quality (%)	Entrainment Mass Flow (lb/s)	Entraiment Percentage of Total Flow
12.87	0.00	0.00
22.02	0.01361	30.62
31.74	0.02391	53.79
41.13	0.02284	51.38
50.53	0.01994	44.86
59.84	0.01645	37.01
69.10	0.01278	28.75
78.25	0.00911	20.50
87.33	0.00519	11.68

Table 3.5 Calculated entrainment mass flow rate and percentage with $f_i = 5 \times f_{iw}$
Outlet pressure : <u>35</u> (psig) , Total mass flow rate : <u>0.04445</u> (lb/s)

Outlet Quality (%)	Entrainment Mass Flow (lb/s)	Entraiment Percentage of Total Flow
10.82	0.00000	00.00
20.49	0.00636	14.31
30.19	0.02047	46.05
39.80	0.02120	47.69
49.31	0.01912	43.01
58.81	0.01579	35.93
68.23	0.01226	27.58
77.64	0.00876	19.71
87.02	0.00522	11.74

Table 3.6 Calculated entrainment mass flow rate and percentage with $f_i = 5 \times f_{iw}$
Outlet pressure : <u>50</u> (psig) , Total mass flow rate : <u>0.04445</u> (lb/s)

Outlet Quality (%)	Entrainment Mass Flow (lb/s)	Entraiment Percentage of Total Flow
9.31	0.00	0.00
18.83	0.00174	3.91
28.57	0.01675	37.68
38.29	0.01940	43.64
48.00	0.01810	40.72
57.59	0.01520	34.20
67.18	0.01186	26.68
76.74	0.00838	18.85
86.28	0.00495	11.14

Table 3.7 Calculated entrainment mass flow rate and percentage with $f_i = 5 \times f_{iw}$
Outlet pressure : <u>500</u> (psia) , Total mass flow rate : <u>0.38472</u> (lb/s)

Outlet Quality (%)	Entrainment Mass Flow (lb/s)	Entraiment Percentage of Total Flow
11.15	0.25196	65.49
23.21	0.25116	65.28
35.26	0.21703	56.41
47.32	0.17794	46.25
59.17	0.13854	36.01
71.27	0.09736	25.31
83.43	0.05535	14.39
95.50	0.01394	3.62

Table 3.8 Calculated entrainment mass flow rate and percentage with $f_i = f_{iW}$.
Outlet pressure : <u>20</u> (psig) , Total mass flow rate : <u>0.04445</u> (lb/s)

Outlet Quality (%)	Entrainment Mass Flow (lb/s)	Entraiment Percentage of Total Flow
12.80	0.0	0.0
22.25	0.00794	17.86
32.55	0.02149	48.35
42.59	0.02118	47.65
52.35	0.01825	41.06
62.88	0.01435	32.28
73.00	0.01050	23.62
83.24	0.00665	14.96
94.29	0.00226	5.08

Table 3.9 Calculated entrainment mass flow rate and percentage with $f_i = f_{iW}$.
Outlet pressure : <u>35</u> (psig) , Total mass flow rate : <u>0.04445</u> (lb/s)

Outlet Quality (%)	Entrainment Mass Flow (lb/s)	Entraiment Percentage of Total Flow
10.91	0.0	0.0
20.59	0.00295	6.64
30.64	0.01645	37.01
40.70	0.01917	43.13
50.66	0.01732	38.97
60.52	0.01400	31.50
70.35	0.01049	23.60
80.20	0.00688	15.48
90.03	0.00344	7.74

Table 3.10 Calculated entrainment mass flow rate and percentage with $f_i = f_{iw}$

Outlet pressure : <u>50</u> (psig) , Total mass flow rate : <u>0.04445</u> (lb/s)

Outlet Quality (%)	Entrainment Mass Flow (lb/s)	Entraiment Percentage of Total Flow
9.65	0.00	0.00
19.10	0.00071	1.60
29.07	0.01175	26.43
39.08	0.01672	37.62
49.07	0.01617	36.38
58.99	0.01331	29.94
68.91	0.01004	22.59
78.83	0.00663	14.92
88.80	0.00321	7.22

Table 3.11 Calculated entrainment mass flow rate and percentage with $f_i = f_{iw}$

Outlet pressure : <u>500</u> (psia) , Total mass flow rate : <u>0.38472</u> (lb/s)

Outlet Quality (%)	Entrainment Mass Flow (lb/s)	Entraiment Percentage of Total Flow
11.15	0.15697	40.80
23.23	0.21934	57.01
35.32	0.20416	53.07
47.40	0.16929	44.00
59.29	0.13061	33.95
71.38	0.09041	23.50
83.48	0.04999	12.99
95.62	0.01069	2.78

Pressure boundary
↓

Boundary node → | 50 |

| 49 |
| 48 |
| 47 |
| . |
| . |
| . |
| 4 |
| 3 |
| 2 |

Node length = 3 in

Boundary node → | 1 |
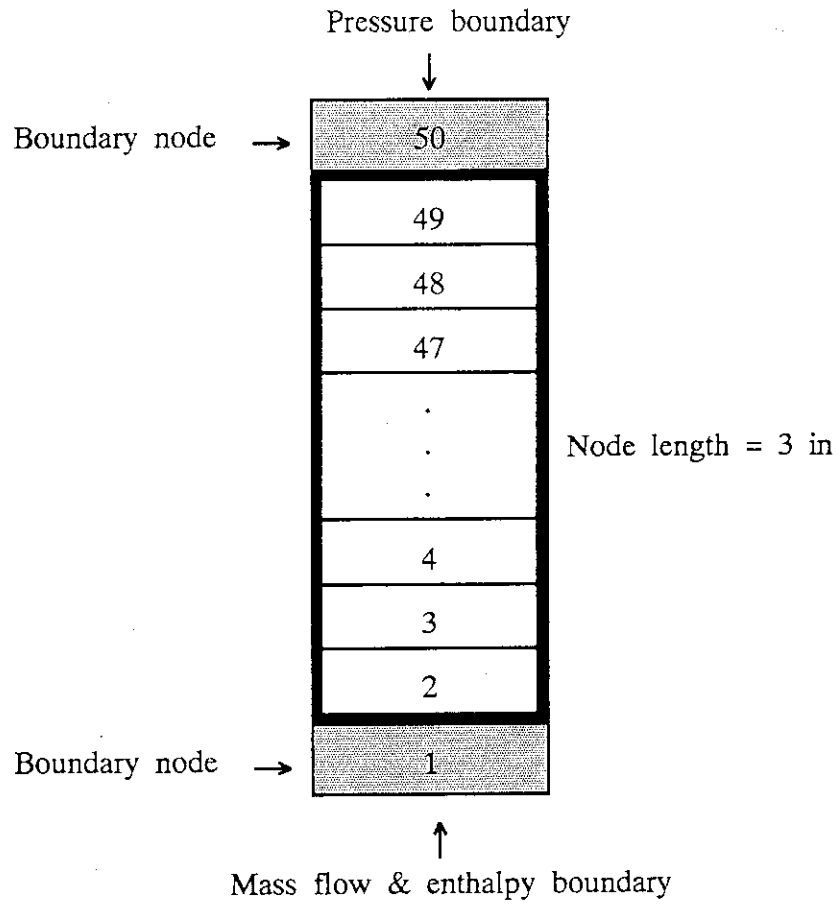
↑
Mass flow & enthalpy boundary

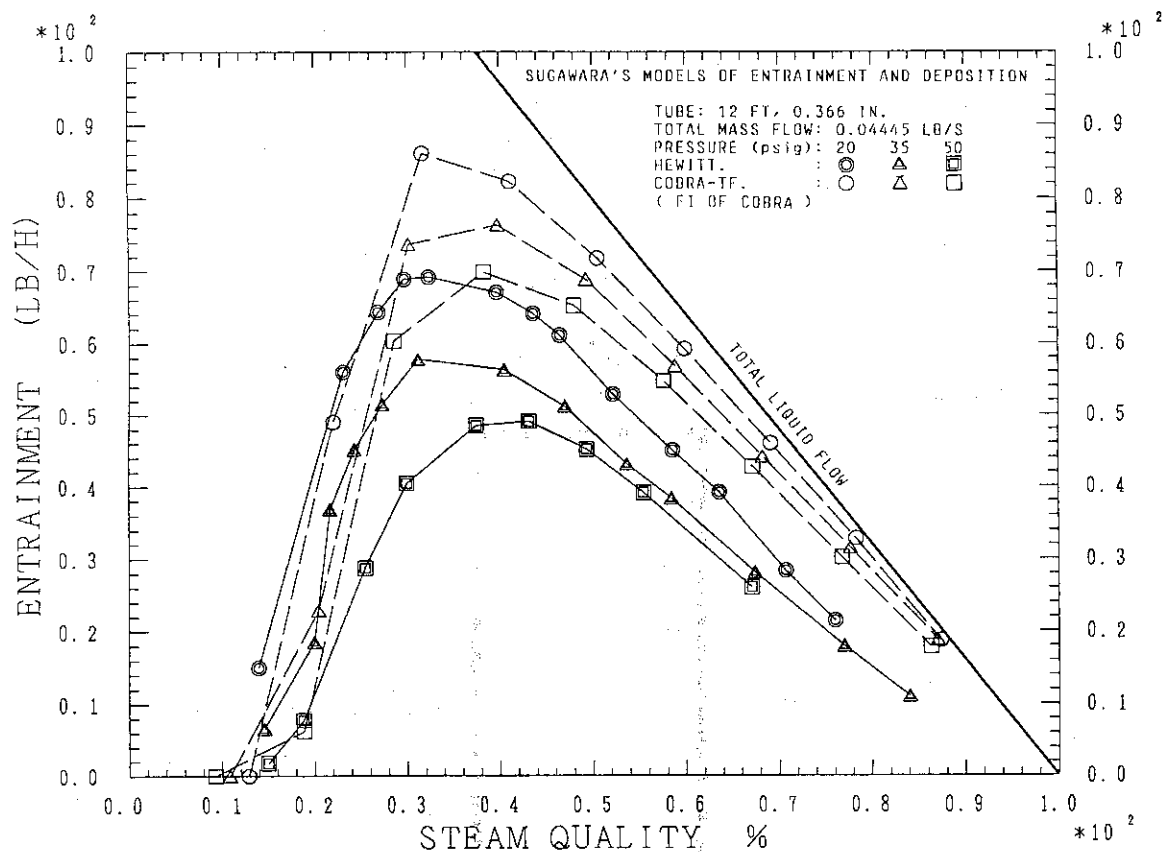Fig. 3.1 Noding diagram for entrainment experiments

Fig. 3.2   Comparisons of entrainment mass flow rate between calculation and experiment for lower pressures with $f_i = 5 \times f_{iW}$
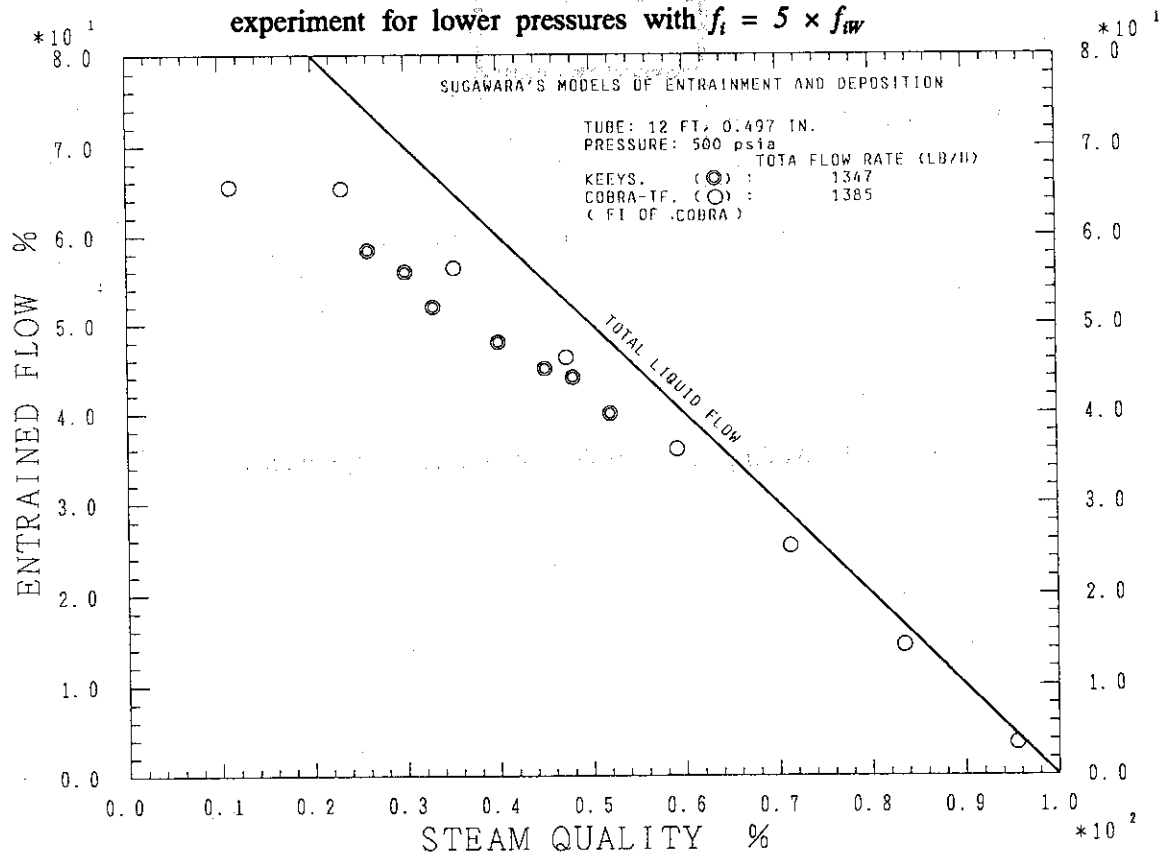

Fig. 3.3   Comparison of entrainment percentage out of total flow between calculation and experiment for 3.4 MPa (500 psia) case with $f_i = 5 \times f_{iW}$
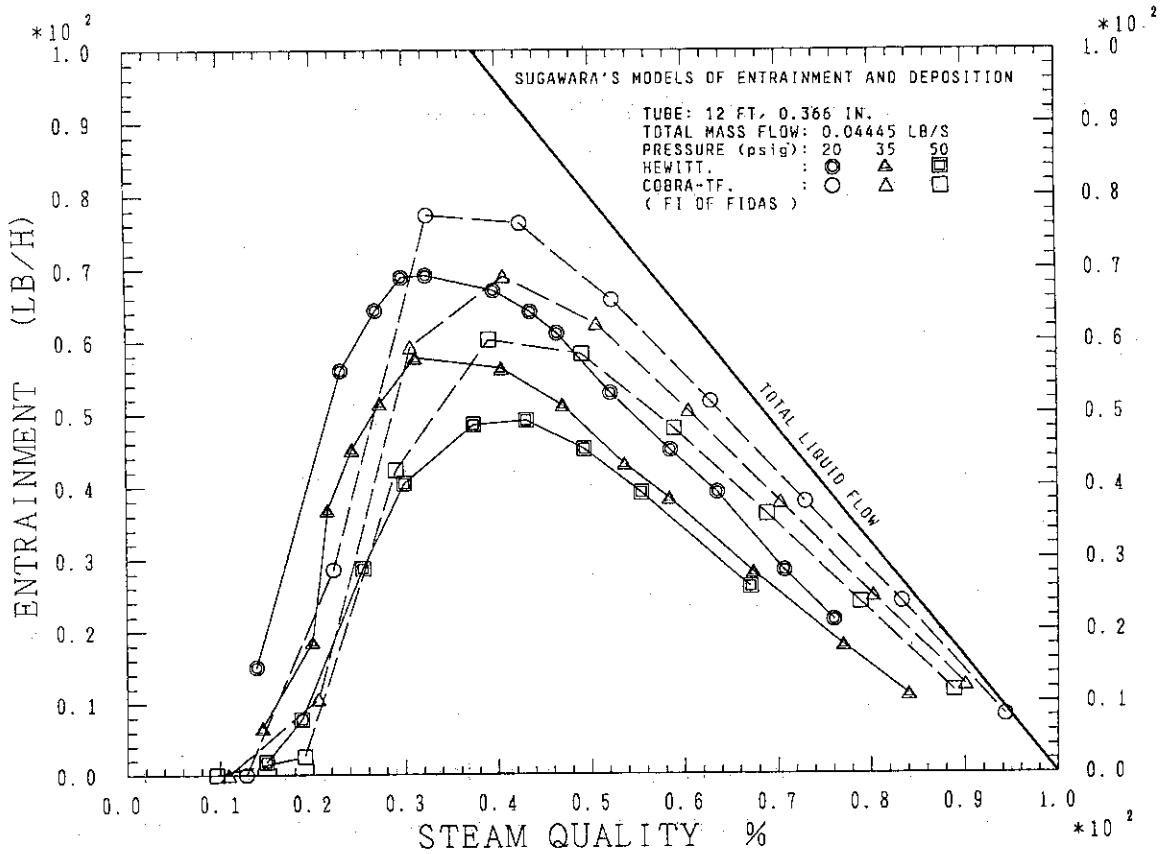
Fig. 3.4 Comparisons of entrainment mass flow rate between calculation and experiment for lower pressures with $f_i = f_{iw}$
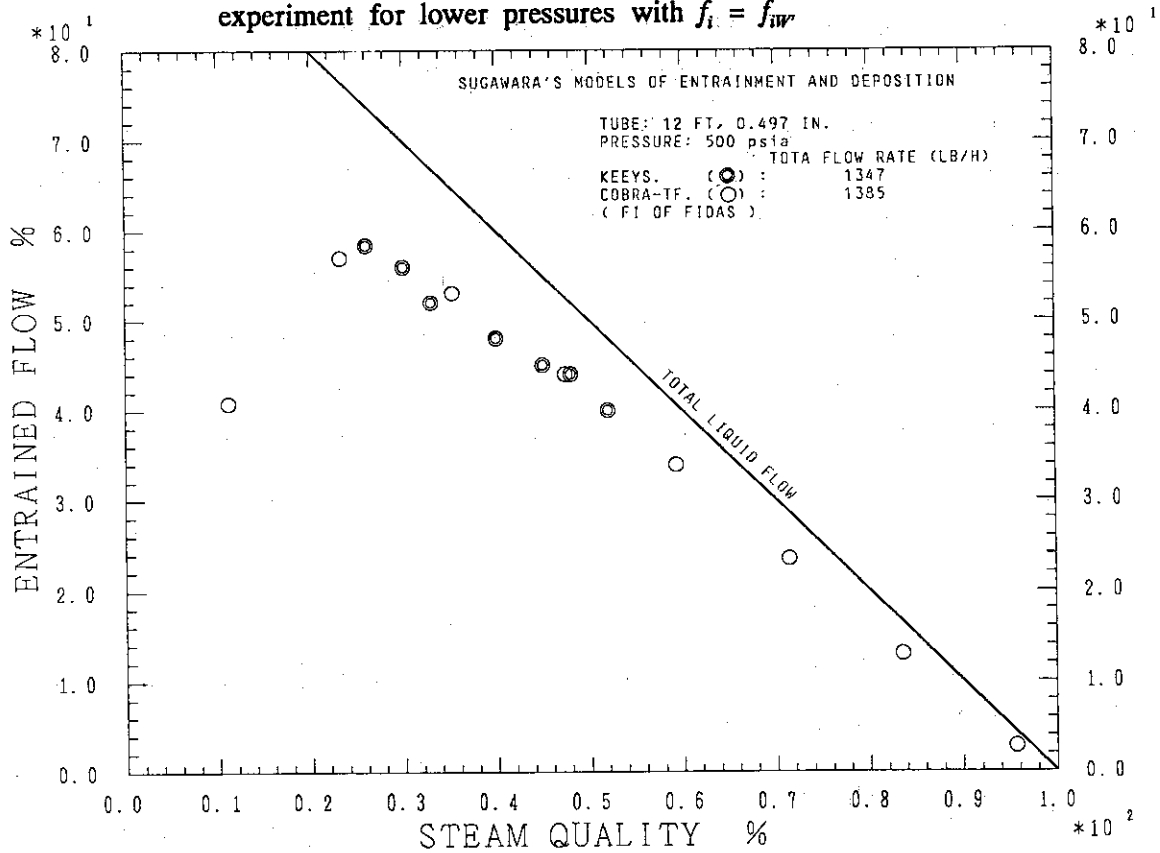

Fig. 3.5 Comparison of entrainment percentage out of total flow between calculation and experiment for 3.4 MPa (500 psia) case with $f_i = f_{iw}$

4. Improvement of Entrainment Model for COBRA-TF

4.1 Derivation of Entrainment Correlation

Based on Würtz correlation[6] expressed by the following dimensionless group,

$$S_w = \left(\frac{\tau_i \times k_s}{\sigma} \right) \times \left(\frac{u_v \times \mu_l}{\sigma \times g} \right) \tag{27}$$

Sugawara proposed[7] the following dimensionless expression in order to take account of the effect of the density :

$$S_s = \left(\frac{\tau_i \times k_s}{\sigma} \right) \times \left(\frac{u_v \times \mu_l}{\sigma \times g} \right) \times \left(\frac{\rho_l}{\rho_v} \right)^{0.4} \tag{28}$$

Entrainment generation rates, $m_{E,\,exp}$, estimated from the experimental data of Hewitt et al.[9] and Keeys et al.[10], which were close to the equilibrium values, are plotted against S_w in Fig. 4.1 and S_s in Fig. 4.2 . In order to estimate the entrainment generation rates, a series of calculations were performed changing the given entrainment generation rate until calculational results agreed well with the experimental data.

Comparison between Figs. 4.1 and 4.2 suggests that the density ratio parameter is not enough to correlate the experimental data and COBRA-TF calculations are more sensitive to other effects, probably the mass flux effects due to the structure of the code.

It is denoted that the droplet entrainment occurs when the retaining force of the liquid film becomes smaller than the interfacial shear force, and the liquid viscous force is probably not negligible as a retaining force even for low viscous fluid. This consideration with the mass flux effects can be represented by a Reynolds number ratio in the following form :

$$\left(\frac{Re_l}{Re_{vl}} \right)^m \tag{29}$$

Re_{vl} is the vapor Reynolds number at the interface between liquid film and vapor, and it is defined by the following expression :

$$Re_{vl} = \frac{u_{vl} \times \rho_v \times D_h \times \alpha_v}{\mu_v} \tag{30}$$

where, μ_v is the vapor viscosity and the other parameters are defined in Eqs.(4), (5) and (17). Therefore, one can obtain the following dimensionless expression :

$$S_z = \left(\frac{\tau_i \times k_s}{\sigma}\right) \times \left(\frac{u_v \times \mu_l}{\sigma \times g}\right) \times \left(\frac{\rho_l}{\rho_v}\right)^{0.4} \times \left(\frac{Re_l}{Re_{vl}}\right)^m \tag{31}$$

Fig. 4.3 shows that the data can be satisfactorily correlated if $m = 0.235$, and hence, the dimensionless group in Eq.(31) becomes :

$$S_z = \left(\frac{\tau_i \times k_s}{\sigma}\right) \times \left(\frac{u_v \times \mu_l}{\sigma \times g}\right) \times \left(\frac{\rho_l}{\rho_v}\right)^{0.4} \times \left(\frac{Re_l}{Re_{vl}}\right)^{0.235} \tag{32}$$

The main reason for the discrepancy shown in the Fig. 4.3 for low pressure data is supposed to be an incorrect extrapolation of the equivalent sand roughness k_s , which was estimated by Würtz in the high pressure range of 3 to 9 MPa. To overcome this discrepancy, an equivalent wave height Δh, which is an accurate value for k_s in Eq.(32), was determined for each data point from comparison between the calculated value using Eq.(32) and the estimated experimental value, as performed by Sugawara[7]. As recognized in Sugawara's results[7] and Ueda's analysis[16], Δh should be a function of the vapor Reynolds number, increasing with the increase of the vapor Reynolds number in the range below 1×10^5. Obtained values for $\Delta h / k_s$ are plotted against the vapor Reynolds number on Fig. 4.4. This shows that k_s should be replaced by Δh, which can be correlated with good accuracy by the following equations:

$$\Delta h = k_s \qquad , \qquad for\ Re_v \geq 1 \times 10^5 \tag{33}$$

$$\Delta h = k_s \times \log_{10}\left[\left(\frac{Re_v}{34028}\right)^{2.39232}\right] , \qquad for\ Re_v < 1 \times 10^5 \tag{34}$$

On Fig. 4.5, the data are plotted against the dimensionless group defined in Eq.(32) but by replacing k_s with Δh given by Eqs.(33) and (34). Finally, from Fig. 4.5, it is shown that the entrainment rate in a wide range of pressure and mass velocity can be correlated by the following correlation:

$$m_E = 0.219 \times \left(\frac{\tau_i \times \Delta h}{\sigma}\right) \times \left(\frac{u_v \times \mu_l}{\sigma \times g}\right) \times \left(\frac{\rho_l}{\rho_v}\right)^{0.4} \times \left(\frac{Re_l}{Re_{vl}}\right)^{0.235} \tag{35}$$

$$\Delta h = k_s \qquad\qquad , \quad for\ Re_v \geq 1 \times 10^5 \tag{36}$$

$$\Delta h = k_s \times \log_{10}\left[\left(\frac{Re_v}{34028}\right)^{2.39232}\right] , \quad for\ Re_v < 1 \times 10^5 \tag{37}$$

4.2 Assessment Calculations with Derived Entrainment Correlation

Calculations were performed by using the above derived entrainment model together with Sugawara's deposition correlation to obtain the entrainment mass flow rate at the test section exit for the simulated experiments. Some instabilities have been observed in the calculations and in order to overcome these instabilities, an approximation was made by substituting the shear stress at the vapor–liquid interface by the shear stress between the liquid film and the wall. This approximation is justified since the liquid film thickness is very small compared to the hydraulic diameter.

The results of entrained liquid mass flow rate and the percentage of the entrainment out of the total flow are summarized in Tables 4.1, 4.2, 4.3, 4.4 and 4.5, for the pressures of 20, 35, 50 psig, 500 and 1000 psia, respectively. These results are plotted with the experimental data against the exit steam quality in Fig. 4.6 for low pressures, and Figs. 4.7 and 4.8 for high pressures. It can be seen in these figures that the calculational results agree well with the experimental data in the dependence of the entrained flow rate on the steam quality, pressure and mass velocity.

4.3 Discussion

Based on the investigation presented above, there factors are found necessary to be added to the Würtz correlation in order to get good predictions by COBRA–TF for a wide range of experimental data. The first factor is to take account of the pressure effect and is represented by the density ratio of liquid to vapor. This density ratio parameter is found to be identical to that in the Sugawara's correlation for entrainment. The second factor is a function of vapor Reynolds number and is expressed by Eq.(37) above. Since the corresponding factor in the Sugawara's correlation (Eq.(22)) can be expressed as follows,

$$\Delta h_{eq} = k_s \times \log_{10}\left[\left(\frac{Re_v}{34028}\right)^{2.136}\right] \tag{38}$$

the present factor is 1.12 (= 2.39232/2.136) times as large as that in Sugawara correlation. The third factor has been newly introduced for COBRA-TF. This factor is a function of both liquid and vapor Reynolds numbers and is considered to include both the liquid viscous effect and the mass flux effect. Some other existing entrainment correlations[17],[18] also have dependency on liquid Reynolds number. Since this is the main difference from the Sugawara's entrainment correlation, more detailed investigation on this is presented in the following.

In order to make the meaning of this factor clear, the same type of information as in Fig. 4.2 is presented in Fig. 4.9 with two additional lines. The dashed line presents the relation of

$$m_{E,exp} = 0.219 \times S_s \tag{39}$$

and is corresponding to the Sugawara's correlation excluding the second factor, which is important only for low pressure cases. The solid line presents a relation of

$$m_{E,exp} = 0.084 \times S_s \tag{40}$$

and can correlate all the low pressure data with considering the second factor and some of the high pressure data. This indicates that the low pressure data can be correlated only with the Sugawara's two factors if the proportional constant is changed from 0.219 to 0.084. In other words, the Sugawara's correlation should be modified when it is used in COBRA-TF because of the differences in the other part of the code related to the entrainment calculation and the modification factor is simply a constant of 0.3836. This also means that the newly introduced third factor $(Re_l/Re_{vl})^{0.235}$ is almost constant for the low pressure cases giving the value around 0.3836 mentioned above. However, for the high pressure cases, this factor tends to increase with decreasing in the steam quality. Therefore, the relation expressed by Eq.(40) cannot correlate all the data both for low and high pressures as recognized in Fig. 4.9, and hence, another relation given by Eq.(35) is necessary to correlate all the data.

Incidentally, for high pressure cases, the agreement was good enough as shown in Fig. 3.5 even with the Sugawara's correlation and there was no need to improve the correlation. As recognized from Fig. 4.9, however, Sugawara correlation is not enough to correlate all the high pressure data and the third factor plays an important role to correlate all of them. This

means that although the correlation is necessary to be modified to correlate all the data, calculated mass flow rates for entrained droplets are not very sensitive to this modification and are almost the same for both of the two correlations at high pressure cases. At low pressures, on the other hand, the calculational results are very sensitive to the differences between the two correlations and the modified one with the third factor gives a good agreement as shown in Fig. 4.6.

Although above discussion gives an explanation for the third factor, the most important point obtained through this study is the mass flow rate of the liquid entrainment is not simply determined by the entrainment and deposition relations. That is, this is a very complicated phenomenon to be calculated and there are many factors to determine the phenomenon. Therefore, if another code system with different constitutive equations, for instance, is used for the prediction of the entrainment/deposition phenomenon, the entrainment and deposition correlations may ought to be modified in order to get good agreement with the experimental data.

Finally, it should be noted the assessment calculations for other experiments be necessary in order to comfirm the general applicability of the new correlation. These calculations will be performed in the near future.

Table 4.1 Calculated entrainment mass flow rate and percentage with new correlation
Outlet pressure : 20 (psig) , Total mass flow rate : 0.04445 (lb/s)

Outlet Quality (%)	Entrainment Mass Flow (lb/s)	Entraiment Percentage of Total Flow
12.82	0.00	0.00
22.34	0.01221	27.47
32.49	0.01872	42.12
42.36	0.01771	39.84
52.08	0.01459	32.82
61.78	0.01119	25.17
71.63	0.00772	17.37
81.17	0.00445	10.01
91.25	0.00102	2.295

Table 4.2 Calculated entrainment mass flow rate and percentage with new correlation
Outlet pressure : 35 (psig) , Total mass flow rate : 0.04445 (lb/s)

Outlet Quality (%)	Entrainment Mass Flow (lb/s)	Entraiment Percentage of Total Flow
10.91	0.00	0.00
20.63	0.00632	14.22
30.64	0.01555	34.98
40.54	0.01578	35.50
50.42	0.01340	30.15
60.23	0.01015	22.83
70.06	0.00696	15.66
79.93	0.00387	8.71
89.97	0.00107	2.41

Table 4.3   Calculated entrainment mass flow rate and percentage with new correlation
Outlet pressure : 50 (psig) ,   Total mass flow rate : 0.04445   (lb/s)

Outlet Quality (%)	Entrainment Mass Flow (lb/s)	Entraiment Percentage of Total Flow
9.54	0.00	0.00
19.12	0.00220	4.95
29.07	0.01260	28.35
38.97	0.01394	31.36
48.91	0.01262	28.39
58.74	0.00926	20.83
68.64	0.00629	15.57
78.56	0.00343	7.72
88.62	0.00109	2.45

Table 4.4   Calculated entrainment mass flow rate and percentage with new correlation
Outlet pressure : 500 (psia) ,   Total mass flow rate : 0.38472   (lb/s)

Outlet Quality (%)	Entrainment Mass Flow (lb/s)	Entraiment Percentage of Total Flow
11.16	0.23551	61.22
23.23	0.22175	57.64
35.31	0.19101	49.65
47.40	0.15444	40.14
59.38	0.11624	30.22
71.58	0.07627	19.83
83.68	0.03756	9.76
95.79	0.00391	1.02

Table 4.5   Calculated entrainment mass flow rate and percentage with new correlation

Outlet pressure : <u>1000</u>   (psia) ,   Total mass flow rate : <u>0.37423</u>   (lb/s)

Outlet Quality (%)	Entrainment Mass Flow (lb/s)	Entraiment Percentage of Total Flow
13.54	0.21727	58.06
25.29	0.20048	53.57
37.04	0.17253	46.10
48.79	0.13947	37.27
60.55	0.10400	27.79
72.31	0.06777	18.11
84.20	0.03195	8.54
95.85	0.00283	0.76

$$S_w = \left(\frac{\tau_i \times k_s}{\sigma}\right) \times \left(\frac{u_v \times \mu_l}{\sigma \times g}\right)$$
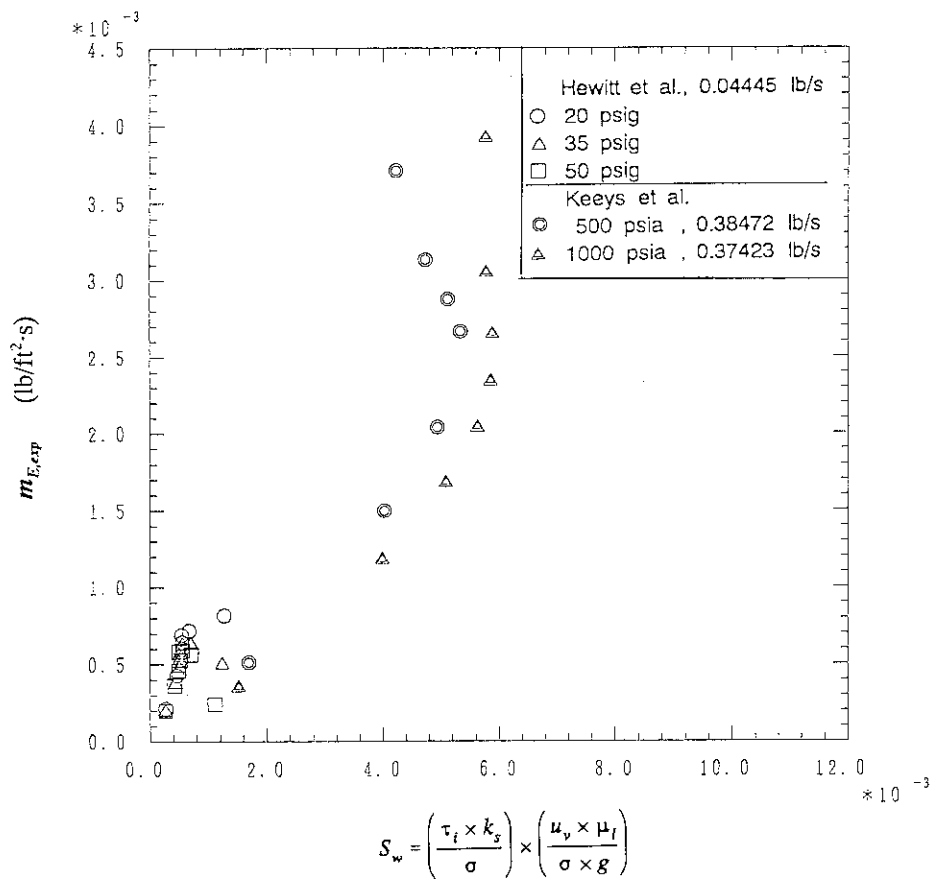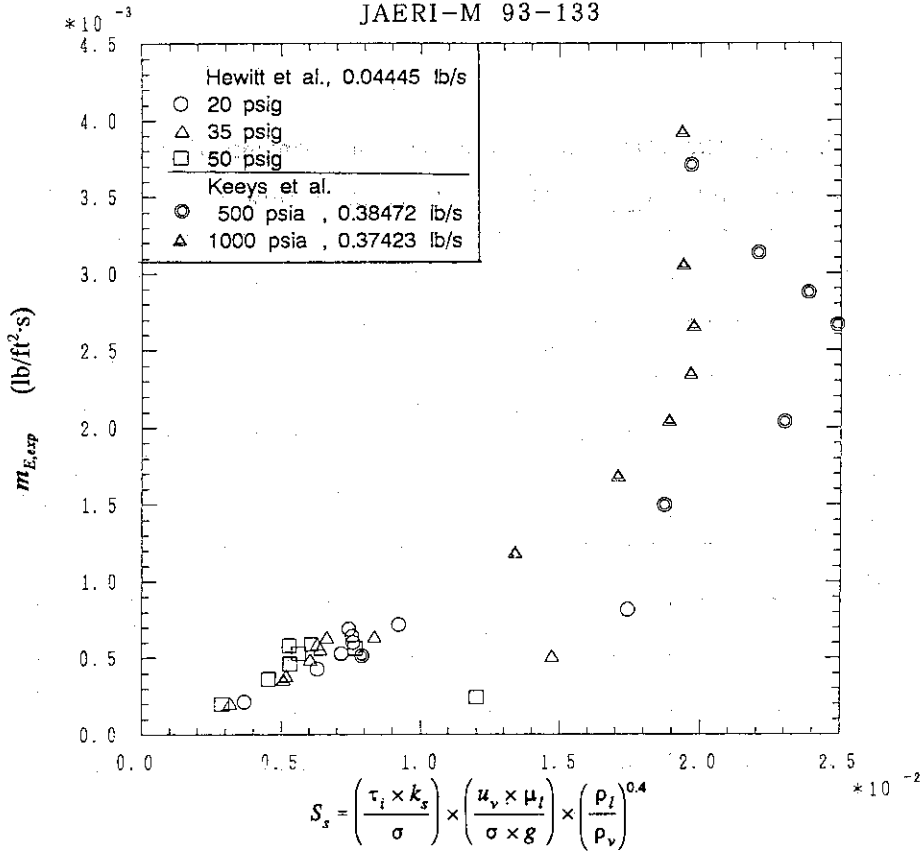
Fig. 4.1   Calculated dimensionless parameter (S_w) versus estimated entrainment generation rate based on experimental data

Fig. 4.2 Calculated dimensionless parameter (S_s) versus estimated entrainment generation rate based on experimental data
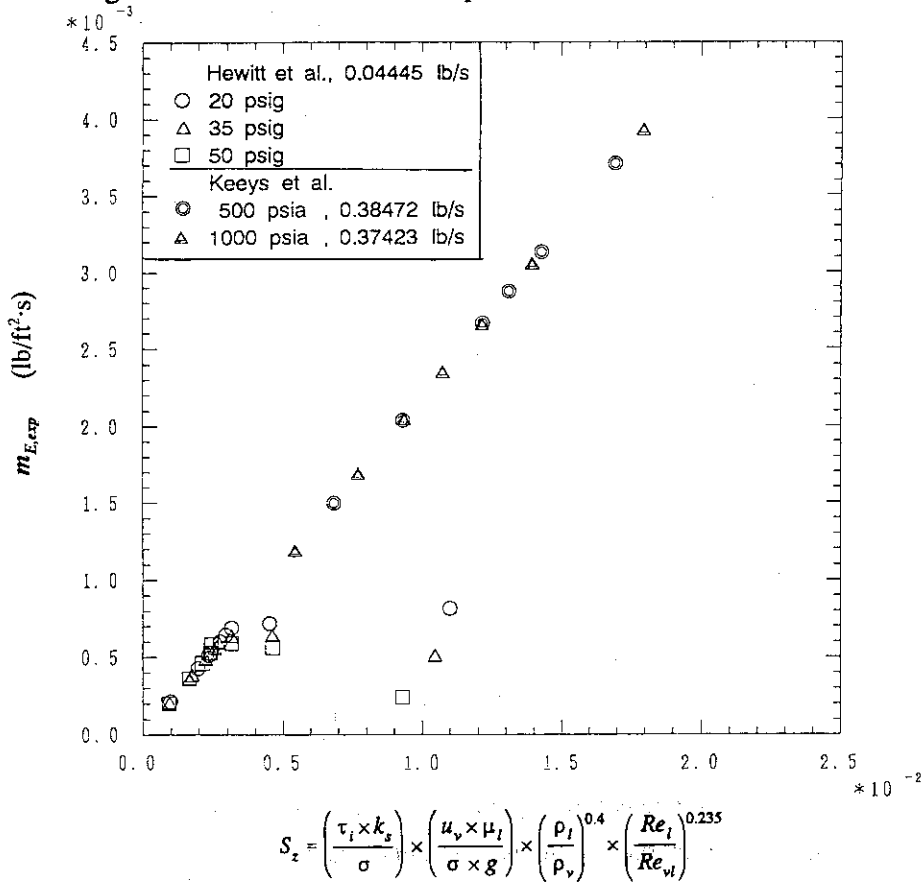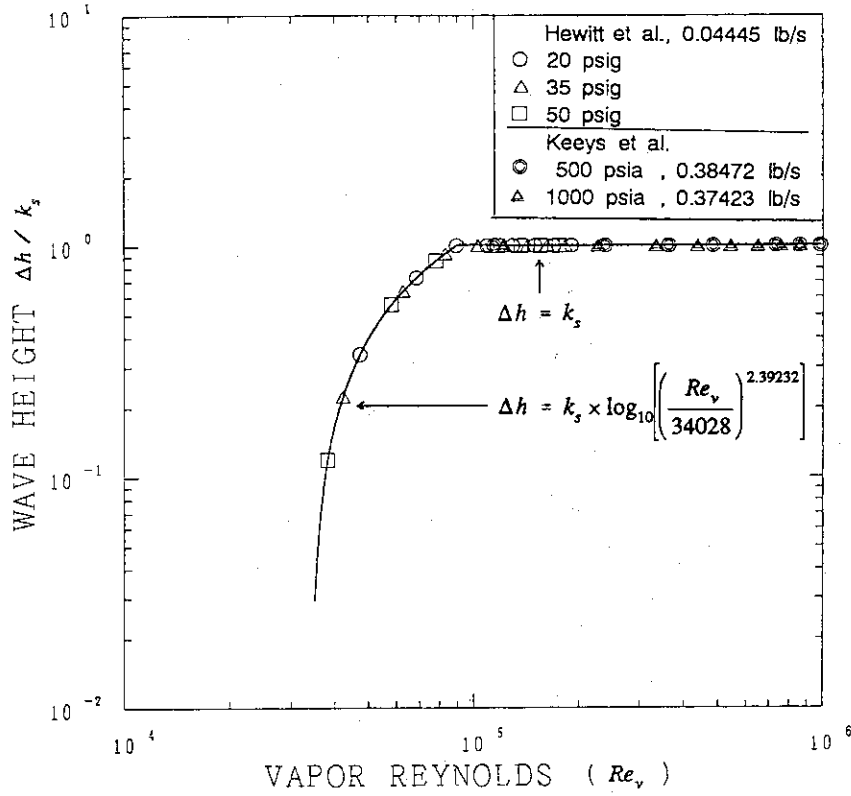
$$S_s = \left(\frac{\tau_i \times k_s}{\sigma}\right) \times \left(\frac{u_v \times \mu_l}{\sigma \times g}\right) \times \left(\frac{\rho_l}{\rho_v}\right)^{0.4}$$

$$S_z = \left(\frac{\tau_i \times k_s}{\sigma}\right) \times \left(\frac{u_v \times \mu_l}{\sigma \times g}\right) \times \left(\frac{\rho_l}{\rho_v}\right)^{0.4} \times \left(\frac{Re_l}{Re_{vl}}\right)^{0.235}$$

Fig. 4.3 Calculated dimensionless parameter (S_z) with k_s versus estimated entrainment generation rate based on experimental data
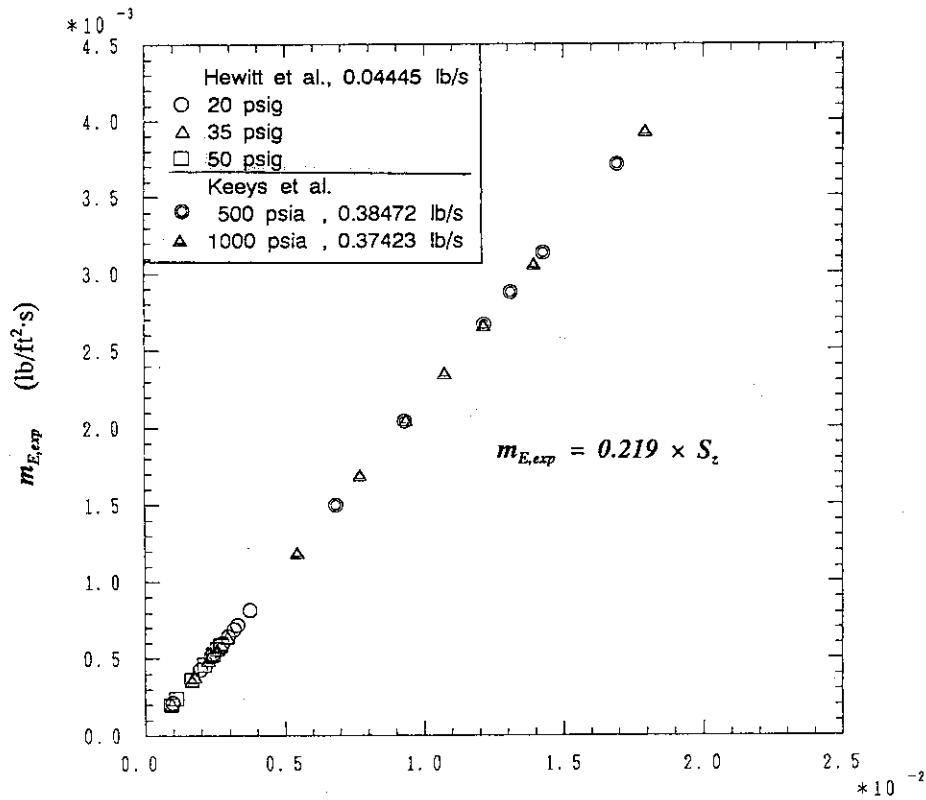
Fig. 4.4 Calculated roll wave height versus vapor Reynolds number for calculation

$$S_z = \left(\frac{\tau_l \times \Delta h}{\sigma}\right) \times \left(\frac{u_v \times \mu_l}{\sigma \times g}\right) \times \left(\frac{\rho_l}{\rho_v}\right)^{0.4} \times \left(\frac{Re_l}{Re_{vl}}\right)^{0.235}$$

Fig. 4.5 Calculated dimensionless parameter (S_z) with Δh versus estimated entrainment generation rate based on experimental data
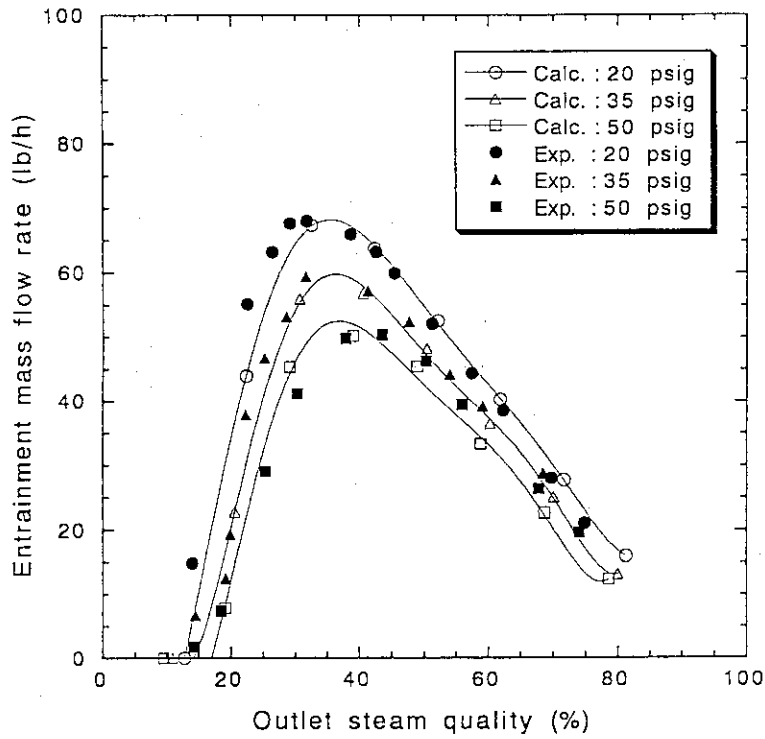
Fig. 4.6   Comparisons of entrainment mass flow rate between calculation
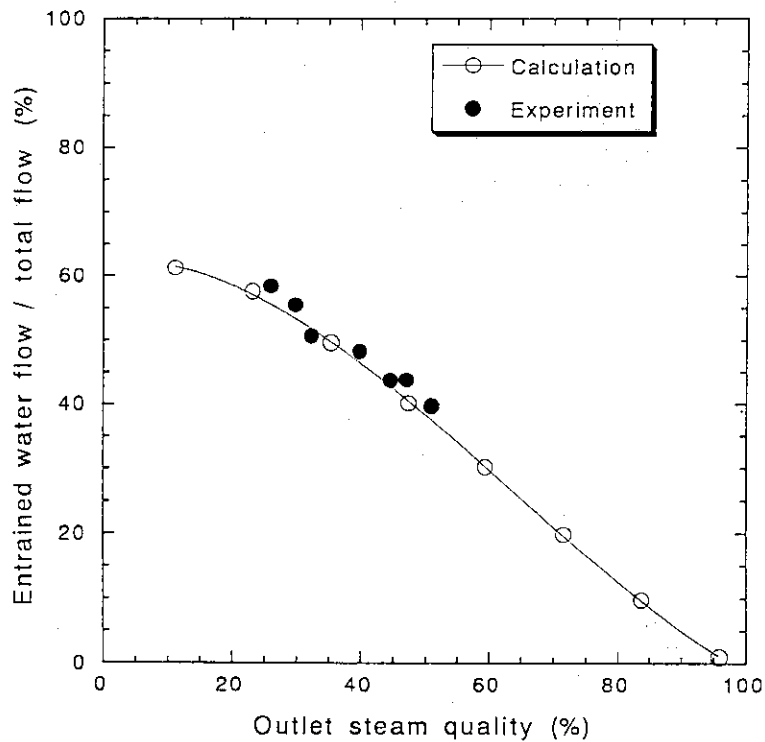and experiment for lower pressures

Fig. 4.7   Comparison of entrainment percentage out of total flow between
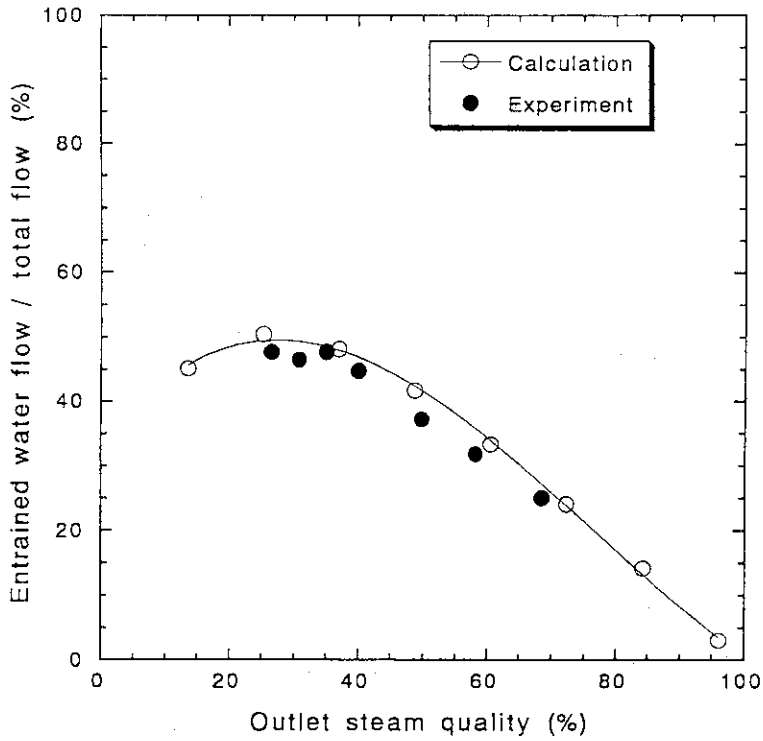calculation and experiment for 3.4 MPa (500 psia) case

Fig. 4.8   Comparison of entrainment percentage out of total flow between calculation and experiment for 6.9 MPa (1000 psia) case
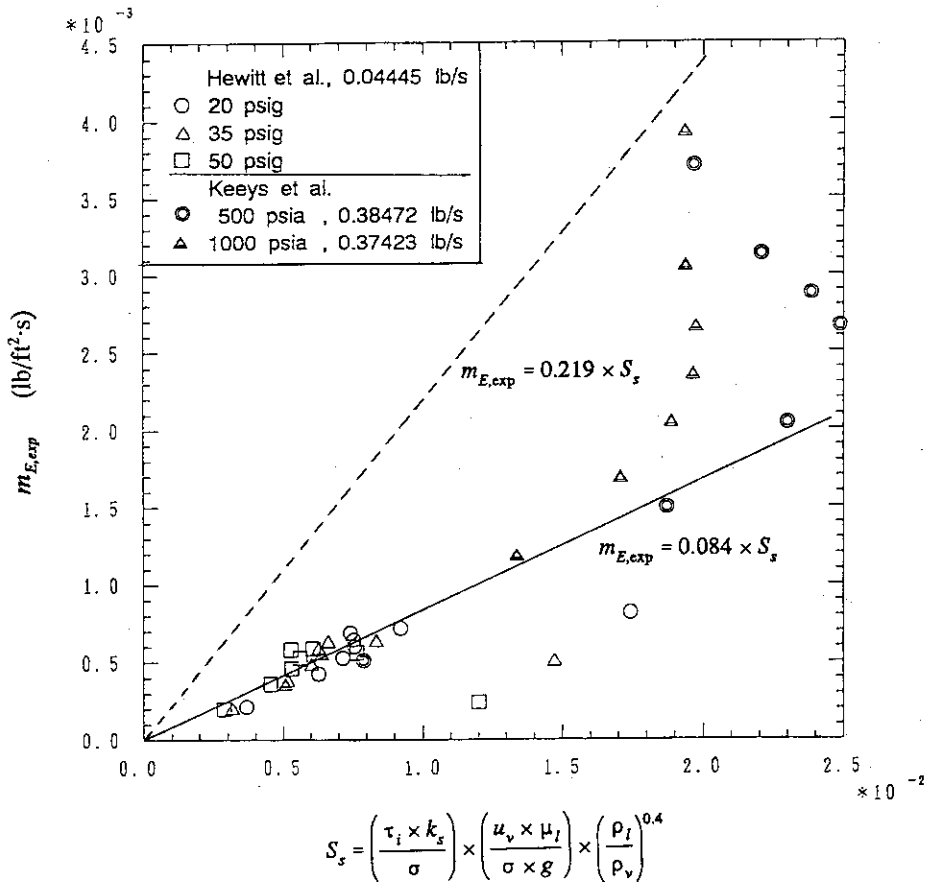

$$S_s = \left(\frac{\tau_i \times k_s}{\sigma}\right) \times \left(\frac{u_v \times \mu_l}{\sigma \times g}\right) \times \left(\frac{\rho_l}{\rho_v}\right)^{0.4}$$

Fig. 4.9   Calculated dimensionless parameter (S_s) versus estimated entrainment generation rate based on experimental data

5. Conclusions

Based on the investigation on the previous studies, correlations for the entrainment and deposition have been changed in the COBRA-TF code in order to improve its predictive capability for the entrainment/deposition phenomenon at low pressures less than 0.5 MPa.

As the first step, Sugawara's correlations for the entrainment and the deposition, which were used in the FIDAS code, were introduced into COBRA-TF. Although calculational results with these became in much better agreement with the concerned experimental data than before, the agreement was not yet satisfactory. Then, as the second step, the correlation for the interfacial friction factor was also changed to the Wallis' and this resulted in some more improvement in the calculational results. However, discrepancies between calculated results and the experimental data were still in the range of about 20 %. That is, it has been found the COBRA-TF code can not well predict the experimental data even with those correlations, with which the FIDAS code can predict them very well. This indicates the entrainment/deposition phenomenon is a very complicated process to be calculated and the phenomenon is not only determined with the entraiment and deposition relations but with many other factors, which are different from code to code.

In order to get a better agreement with the experimental data, a new entrainment correlation has been derived based on the Würtz's correlation and the Sugawara's ideas for modification factors. The new correlation has one more factor than the Sugawara's and this factor is a function of two Reynolds numbers for the liquid film and the relative motion between the vapor and the liquid film. The calculated results with the new entrainment correlation together with the Sugawara's deposition correlation and the Wallis' interfacial friction factor correlation are in very good agreement with the experimental data in a wide range of flow conditions, indicating a significant improvement on the predictive capability of COBRA-TF for the entrainment/deposition phenomenon.

Acknowledgements

5. Conclusions

Based on the investigation on the previous studies, correlations for the entrainment and deposition have been changed in the COBRA-TF code in order to improve its predictive capability for the entrainment/deposition phenomenon at low pressures less than 0.5 MPa.

As the first step, Sugawara's correlations for the entrainment and the deposition, which were used in the FIDAS code, were introduced into COBRA-TF. Although calculational results with these became in much better agreement with the concerned experimental data than before, the agreement was not yet satisfactory. Then, as the second step, the correlation for the interfacial friction factor was also changed to the Wallis' and this resulted in some more improvement in the calculational results. However, discrepancies between calculated results and the experimental data were still in the range of about 20 %. That is, it has been found the COBRA-TF code can not well predict the experimental data even with those correlations, with which the FIDAS code can predict them very well. This indicates the entrainment/deposition phenomenon is a very complicated process to be calculated and the phenomenon is not only determined with the entraiment and deposition relations but with many other factors, which are different from code to code.

In order to get a better agreement with the experimental data, a new entrainment correlation has been derived based on the Würtz's correlation and the Sugawara's ideas for modification factors. The new correlation has one more factor than the Sugawara's and this factor is a function of two Reynolds numbers for the liquid film and the relative motion between the vapor and the liquid film. The calculated results with the new entrainment correlation together with the Sugawara's deposition correlation and the Wallis' interfacial friction factor correlation are in very good agreement with the experimental data in a wide range of flow conditions, indicating a significant improvement on the predictive capability of COBRA-TF for the entrainment/deposition phenomenon.

Acknowledgements

References

1. Thurgood, M.J. et al. : "COBRA/TRAC – A Thermal–Hydraulics Code for Transient Analysis of Nuclear Reactor Vessels and Primary Coolant Systems", NUREG/CR–3046 (1983).

2. Wheeler, C.L. et al. : "COBRA–IV–I An Interim Version of COBRA for Thermal–Hydraulic Analysis of Rod Bundle Nuclear Fuel Elements and Cores", BNWL–1962 (1976).

3. Rowe, D.S. : "COBRA–IIIC A Digital Computer Program for Steady–State and Transient Thermal–Hydraulic Analysis of Rod Bundle Nuclear Fuel Elements", BNWL–1695 (1973).

4. Hewitt G.F., Hall–Taylor N.S. : "Annular Two–Phase Flow", Pergamon Press, Oxford, (1970).

5. Okubo T., Ezzidi A. and Murao Y. : "Assessment of Models in COBRA–TF Code for Liquid Entrainments in Film–Mist Flow", JAERI–M 93–069 (1993).

6. Würtz, J. : "An Experimental and Theoretical Investigation of Annular Steam–Water Flow in Tubes and Annuli at 30 to 90 Bar", RISO Report No. 372 (1978).

7. Sugawara, S. : "Droplet Deposition and Entrainment Modeling Based on the Three–Fluid Model", Nucl. Eng. Des., 122, 67–84 (1990).

8. Sugawara, S., Miyamoto, Y. : "FIDAS : Detailed Subchannel Analysis Code Based on the Three–Fluid and Three–Field Model", Nucl. Eng. Des., 120, 147–161 (1990).

9. Hewitt, G.F., Pulling, D.J. : "Liquid Entrainment in Adiabatic Steam–Water Flow", AERE–R 5374 (1969).

10. Keeys, R.K.F. et al. : "Liquid Entrainment in Adiabatic Steam–Water Flow at 500 and 1000 p.s.i.a (3.447 and 6.894 x 10^6 N/m^2)", AERE–R 6293 (1970).

11. Wallis G.B. : "One–Dimensional Two–Phase Flow", McGraw–Hill, New York, (1969).

12. Henstock, W.H., Hanratty, T.J. : "The Interfacial Drag and the Height of the Wall Layer in Annular Flows", AIChE J., 22[6], 990–1000 (1976)

13. Tatterson D.F. et al. : "Drop Sizes in Annular Gas–Liquid Flows", AIChE J., 23[1], 68–76 (1977).

14. Cousins L.B. et al. : "Liquid Mass Transfer in Annular Two–Phase Flow", AERE–R 4926 (1965).

15. Whalley P.B. : "The Calculation of Dryout in a Rod Bundle", Int. J. Multiphase Flow, 3, 501–515 (1977).

16. Ueda T. : "Droplet Entrainment Rate and Droplet Diameter in Annular Two-phase Flow", *Trans. JSME* **45**[389], 127-135 (1979) [in Japanese].

17. Ishii M. and Mishima K. : "Correlation for Liquid Entrainment in Annular Two-Phase Flow of Low Viscous Fluid", ANL/RAS/LWR 81-2 (1981).

18. Kataoka I. and Ishii M. : "Mechanism and Correlation of Droplet Entrainment and Deposition in Annular Two-Phase Flow", NUREG/CR-2885(ANL-82-44) (1982).

Nomenclature

d : droplet diameter (ft)

f : friction factor

g : acceleration of gravity (ft/s^2)

k_D : mass transfer coefficient (ft/s)

k_s : equivalent sand roughness (ft)

m_{DE} : deposition rate (lb/ft^{2}s)

m_E : entrainment generation rate (lb/ft^{2}s)

C : mean droplet concentration (lb/ft^3)

D : diameter (ft)

D_h : hydraulic diameter (ft)

Pr : Prandtl number

P_w : wetted perimeter (ft)

Re : Reynolds number

S_{DE} : deposition rate (lb/s)

S_E : entrainment generation rate (lb/s)

Sc : Schmidt number

u : axial velocity (ft/s)

α : volume fraction

δ_{th} : theoretical film thickness (ft)

μ : dynamic viscosity (lb/ft·s)

σ : surface tension of water (lb$_f$/ft)

τ : shear stress (lb$_f$/ft^2)

ρ : density (lb/ft^3)

Δh : hydrodynamic equivalent wave height (ft)

Δh_{eq} : Sugawara's hydrodynamic equivalent wave height (ft)

Δx : axial mesh length (ft)

subscript

e : entrainment

eq : equilibrium

i : vapor–liquid interface

l : liquid

v : vapor

vl : relative value between vapor and liquid